Dai, H. K., Huang, W., Fu, L., Lin, C-H., Wei, D., Dong, Z., You, R., and Chen, C. 2021. Investigation of pressure drop in flexible ventilation ducts under different compression ratios and bending angles. ***Building Simulation***, 14: 1251-61.

Investigation of Pressure Drop in Flexible Ventilation Ducts under Different Compression Ratios and Bending Angles

Ho Kam Dai[1], Wenjie Huang[1], Liye Fu[2], Chao-Hsin Lin[3], Daniel Wei[4], Zhongzhe Dong[4], Ruoyu You[2], Chun Chen[1,5,*]

[1] Department of Mechanical and Automation Engineering, The Chinese University of Hong Kong, Shatin, N.T. 999077, Hong Kong SAR, China
[2] Department of Building Services Engineering, The Hong Kong Polytechnic University, Kowloon, 999077, Hong Kong SAR, China
[3] Environmental Control Systems, Boeing Commercial Airplanes, Everett, WA 98203, USA
[4] Boeing Research & Technology, Beijing 100027, China
[5] Shenzhen Research Institute, The Chinese University of Hong Kong, Shenzhen 518057, China

[*]Email: chunchen@mae.cuhk.edu.hk

Abstract

Due to the large degree of freedom in terms of design and installation, flexible ventilation ducts are commonly used in ventilation systems. However, excessive use of flexible ducts may lead to greater pressure drop and higher energy consumption. This study conducted experimental measurements to characterize the pressure drop in flexible ventilation ducts with different compression ratios and bending angles. This investigation first measured the pressure drop in straight flexible ducts with four compression ratios under various airflow rates. The calculated friction factor for the straight flexible ducts was negatively associated with the compression ratio. Next, the pressure drops in single-bend flexible ducts with various bending angles from 30° to 150° were measured under various airflow rates. The calculated loss coefficient of the bend increased with the bending angle for single-bend flexible ducts. Finally, the influence of the intermediate duct length on the pressure drop across two bends was experimentally investigated. When the length of the intermediate duct was greater than eight times the inner diameter, the pressure drop across a double-bend flexible duct could be calculated from the friction factors and loss coefficients with a relative error less than 1%. The data obtained in this study can be used to calculate the total pressure loss in flexible ventilation ducting systems in buildings.

Keywords: Ventilation, Pressure loss, Flex duct, Fan energy, Friction factor, Loss coefficient.

1. Introduction

Flexible ducts are alternatives to regular rigid ducts for heating, ventilation, and air-conditioning (HVAC) systems in buildings or transportation vehicles. For example, in buildings, the space for running the ducts from the trunk to the branch outlets in the HVAC systems can be very limited due to the wiring or piping already installed. In commercial airplanes, the space for the ventilation ducting system is also very limited and complex in geometry due to the compact aircraft design. Under such circumstances, flexible ducts tend to be a better choice because of their flexibility in design and installation. However, the pressure loss in flexible ducts tends to be higher than that in traditional rigid ducts (Hodges et al. 2013; Kulkarni et al. 2015; Culp 2011; Weaver et al. 2007; Culp et al. 2009; Kokayko et al. 1996; Abushakra et al. 2004; Ojima 2017; Paruchuri et al. 2018), which would lead to greater energy costs for fan operation. Moreover, because of their flexibility, the installation of flexible ducts tends to result in complex ducting-system geometry with unnecessary bends. This would increase the difficulty of predicting the air pressure distribution in these ducts. It is worthwhile to understand the characteristics of pressure drop in flexible ventilation ducts in order to improve their design and installation.

For regular rigid ducts, a large amount of experimental and simulation data on pressure drop has been reported in the literature (Griggs et al. 1987; Huebscher 1948; Griggs et al. 1992; Townsend et al. 1996; Chen et al. 2016). For example, Sun et al. (2015) measured the pressure loss coefficients for 48 flat oval converging and diverging fittings and developed empirical equations for the fittings. Nalla et al. (2012) measured the branch and main loss coefficients for round saddle taps in both diverging and converging flows. Mylaram et al. (2005) conducted experimental measurements to determine the loss coefficients for six different single elbows and a pair of identical elbows in a close-coupled configuration. Salehi et al. (2017) used computational fluid dynamics (CFD) to predict the pressure drop in U-shaped and Z-shaped close-coupled elbows. These studies have provided great insight into the characteristics of pressure loss in regular rigid ducts.

For flexible ducts, probably because of the higher degree of complexity, the relevant studies available in the literature (Hodges et al. 2013; Kulkarni et al. 2015; Culp 2011) are fewer than those for regular rigid ducts. Weaver et al. (2007) and Culp et al. (2009) experimentally measured the pressure losses in three fully stretched flexible ducts with different diameters. Kokayko et al. (1996) found that the pressure loss in a flexible duct in the relaxed position was greater than that in a stretched flexible duct. Abushakra et al. (2004) reported that a compressed flexible duct had a greater pressure drop per unit length than a fully stretched duct. Paruchuri et al. (2018) investigated the influence of sizing on the total pressure loss in a flexible ducting system. Kulkarni et al. (2009) and Gibbs et al. (2010) measured the average absolute roughness of corrugated spiral ducts and included them in the “medium rough” duct roughness category as defined by ASHRAE (2005). Du et al. (2020) experimentally and numerically investigated the effect of bending angle on pressure drop and flow behavior in a corrugated duct under a fully developed flow condition. These studies have enhanced our understanding of pressure

loss in flexible ducts. However, the research is far from complete, as the pressure drop characteristics in flexible ducts with a greater variation in compression ratio and bending angle are still unclear.

Therefore, this study aimed to conduct experimental measurements to characterize the pressure drop in flexible ventilation ducts covering wide ranges of compression ratio and bending angle. This investigation first measured the pressure drop in straight flexible ducts with four compression ratios under various airflow rates. The friction factors were then obtained and correlated with the compression ratio for straight flexible ducts. The pressure drops in single-bend flexible ducts with various bending angles from 30° to 150° were measured under various airflow rates. The loss coefficients of the bends were then calculated. Finally, the influence of intermediate duct length on the pressure drop across two bends was experimentally investigated. The data obtained in this study can be used for the calculations of total pressure loss in flexible ventilation ducting systems in buildings.

2. Methods

2.1 Straight flexible duct

This study first conducted experimental measurements of the pressure drop in straight flexible ducts. Figure 1(a) provides a schematic of the test rig for measuring the pressure drop according to ANSI/ASHRAE standard 120-2017 (American Society of Heating, Refrigeration and Air-Conditioning Engineers, 2017). A centrifugal fan with a variable-speed controller was used to provide various airflow rates. The pressure differential between the upstream (Plane 1) and downstream (Plane 2) regions, $\Delta p_{straight,1-2}$, was measured under different airflow rates using a manometer (Fluke 922, Fluke, UK) with a resolution of 1 Pa. To ensure that the turbulent airflow was fully developed, the length of the upstream duct section was set at $15D$, where D is the inner diameter of the duct. Furthermore, the length of the measured duct section was set at $25D$, while that of the downstream section was set at $4D$, in accordance with ANSI/ASHRAE standard 120-2017 (American Society of Heating, Refrigeration and Air-Conditioning Engineers, 2017). The tracer-gas approach was applied to measure the airflow rate as illustrated in Figure 1(b). Sulfur hexafluoride (SF_6) was used as the tracer gas, and it was steadily released from a cylinder as 1% SF_6 in N_2, into the upstream duct. The SF_6/N_2 injection flow rate, Q_{SF6}, was measured using a flow meter (LZB-6WB, Changzhou Chengfeng Flowmeter Co., Ltd, China). The SF_6 concentration in the downstream region, $C_{SF6,down}$, was measured using a multi-gas monitor (B&K 1302, Bruel & Kjaer, Denmark). According to mass balance, the volumetric airflow rate, Q, can then be calculated by:

$$Q = \frac{C_{SF6,cylinder}}{C_{SF6,down}} Q_{SF6} \qquad (1)$$

where $C_{SF6,cylinder}$ is the SF_6 concentration in the cylinder.

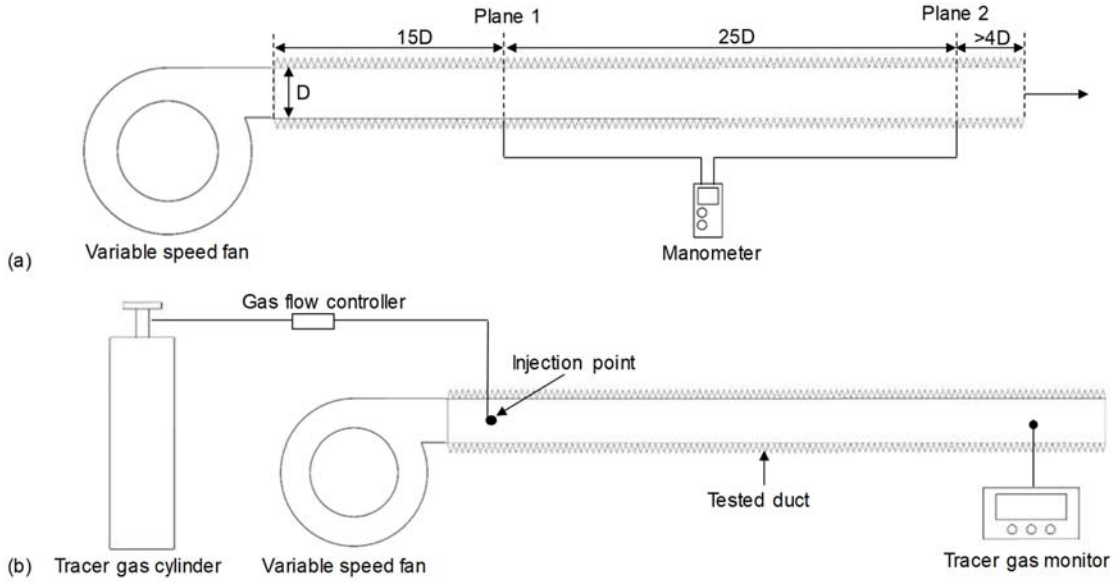

Figure 1. Schematic of the experimental setup for measuring (a) the pressure drop and (b) the airflow rate in a straight flexible duct.

With the measured pressure drop and airflow rate, the friction factor, f, for the straight flexible can be calculated by (Brown 2002):

$$\Delta p_{straight,1-2} = f\frac{L}{D}\frac{\rho}{2}\left(\frac{Q}{A}\right)^2 = f\frac{L}{D}\cdot p_v \qquad (2)$$

where L is the length of the measured duct section ($25D$ in this study), ρ is the air density, A is the inner cross-sectional area of the duct, and p_v is the dynamic pressure in the fully developed turbulent airflow in the straight duct. The pressure drop was measured under various airflow rates (the average air velocity, defined as $V = Q/A$, ranged from 4 to 12 m/s). A least squares regression was performed to obtain the overall friction factor. Note that the friction factor represents the dimensionless air resistance of the straight flexible duct.

By its nature, a flexible duct can be easily compressed and extended. To better understand the air resistance characteristics, this study measured the pressure drop in flexible ducts with different compression and extension scenarios. The compression ratio, R, was defined as the ratio of the actual duct length, L, to the length when the duct was fully stretched, $L_{stretched}$:

$$\mathrm{R} = \frac{L}{L_{stretched}} \qquad (3)$$

Figure 2 displays photographic images of a tested flexible duct with an inner diameter of 52 mm that is fully compressed, in the relaxed position, and fully stretched, respectively. The corresponding compression ratios were 0.8, 0.854, and 1. It can be seen that the compression ratio significantly influenced the geometry of the peaks and valleys, which would further alter the air resistance. Table 1 provides information about test-case setup for measuring the pressure drop in straight flexible ducts. Flexible ducts with inner diameters of 52 and 36 mm, respectively, were tested under various air velocities ranging from 4 to 12 m/s. Four compression ratios from fully stretched to fully compressed were investigated. Each case was repeated three times to ensure repeatability.

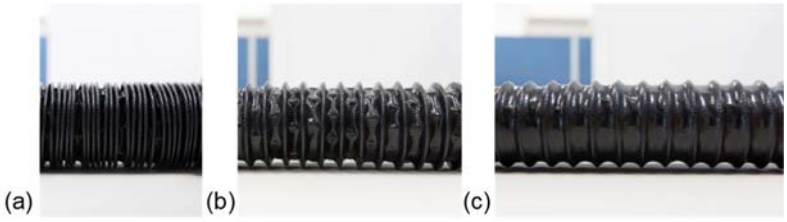

Figure 2. Photographic images of a tested flexible duct that was (a) fully compressed, (b) in the relaxed position, and (c) fully stretched.

Table 1. Case setup for straight flexible ducts.

Case No.	Duct inner diameter, $\boldsymbol{D}$ (mm)	Average air velocity, $\boldsymbol{V = Q/A}$ (m/s)	Compression ratio, $\boldsymbol{R}$	Remark
1	52	4 to 12	1.000	Fully stretched
2	52	4 to 12	0.854	Relaxed position
3	52	4 to 12	0.820	--
4	52	4 to 12	0.800	Fully compressed
5	36	4 to 12	1.000	Fully stretched
6	36	4 to 12	0.950	--
7	36	4 to 12	0.916	Relaxed position
8	36	4 to 12	0.880	Fully compressed

2.2 Bent flexible duct

This study further conducted measurements of pressure drop in bent flexible ducts. Figure 3 shows the experimental setup for these measurements. Planes 1 and 2 were the entrance and exit planes of the bend, respectively. Directly measuring the pressure differential between Plane 1 and 2 would have led to significant errors, as the airflow distribution there was extremely complex. Therefore, the pressure differential between Planes 3 and 4, $\Delta p_{t,3-4}$, was measured instead, as shown in Figure 3. Plane 3 was at a distance of $1.5D$ before Plane 1, while Plane 4 was located $14D$ after Plane 2. This setup ensured that the airflow distribution at the measurement planes was similar to that in a straight duct. Furthermore, to ensure fully

developed turbulent flow, the length of the duct section before Plane 3 was set at $15D$. The airflow rate was measured using the SF_6 tracer-gas method.

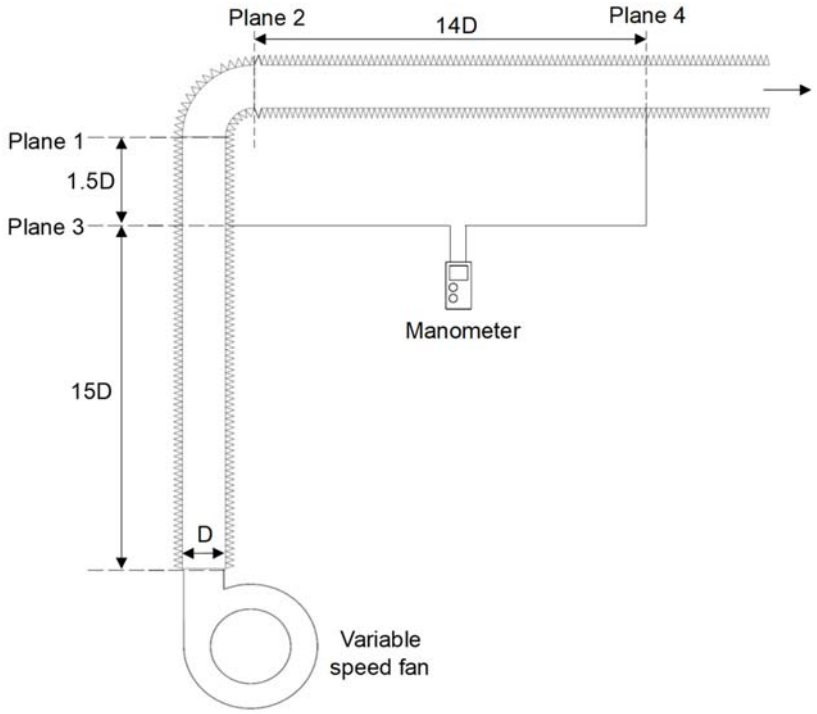

Figure 3. Schematic of the experimental setup for measuring the pressure drop in a bent flexible duct.

The pressure differential across the bend, i.e., $\Delta p_{t,1-2}$, can be calculated by (Brown 2002):

$$\Delta p_{t,1-2} = \Delta p_{t,3-4} - (L_{3-1} + L_{2-4}) \frac{f}{D} \frac{\rho}{2} \left(\frac{Q}{A}\right)^2 \qquad (4)$$

where L_{3-1} is the duct length between Planes 3 and 1, L_{2-4} is the duct length between Planes 2 and 4, and f is the friction factor obtained from the straight flexible duct measurements. With the calculated pressure differential across the bend, the pressure loss coefficient, C, of the bend can be obtained by:

$$\Delta p_{t,1-2} = \mathrm{C} \cdot p_v = \mathrm{C} \cdot \frac{\rho}{2} \left(\frac{Q}{A}\right)^2 \qquad (5)$$

The pressure drop was measured under various airflow rates. A least squares regression was then performed to obtain the overall loss coefficient of the bend.

Table 2 provides information about the case setup for bent flexible ducts with inner diameters of 52 and 36 mm, respectively. The tests were conducted when the flexible ducts were in the relaxed position as the bends could hardly be compressed or stretched. The pressure drop was measured under various average air velocities ranging from 4 to 10 m/s. The tested bending angles ranged from 30° to 150°, and the radius of the bend was 52 and 36 mm, respectively, for the two flexible ducts. Wooden templates with the tested angles were used to hold the upstream and downstream duct sections in the required positions. Each case was repeated three times to ensure repeatability.

Table 2. Case setup for the bent flexible ducts.

Case No.	Duct inner diameter, $\boldsymbol{D}$ (mm)	Average air velocity, $\boldsymbol{V = Q/A}$ (m/s)	Bending angle (°)
1	52	4 to 10	30
2	52	4 to 10	60
3	52	4 to 10	90
4	52	4 to 10	120
5	52	4 to 10	150
6	36	4 to 10	30
7	36	4 to 10	90
8	36	4 to 10	150

2.3 Double-bend flexible duct

With the friction factors for straight flexible ducts and the loss coefficients of the bends, the total pressure drop in a flexible ducting system can be calculated accordingly. However, if the duct length between two bends is too short, the complex airflow distribution may affect the pressure loss. In that case, the two bends and the intermediate duct section should be considered as a whole resistance component. Therefore, this study experimentally investigated the influence of the intermediate duct length on the pressure drop across a double-bend flexible duct. Figure 4 shows the experimental setup for measuring the pressure drop across a duct for which both bending angles are 90°. Plane 1 was the entrance plane of the first bend, and Plane 2 was the exit plane of the second bend. Similar to the single-bend cases, the pressure differential between Planes 3 and 4, $\Delta p_{t,3-4}$, was measured. Plane 3 was at a distance of $1.5D$ before Plane 1, while Plane 4 was located $14D$ after Plane 2. The pressure differentials for the double-bend flexible duct with various intermediate duct lengths were measured. The pressure differential across the double bends, i.e., $\Delta p_{t,1-2}$, was then calculated using Eq. (4). The loss coefficient of the double bends with the intermediate duct as a whole resistance component, $C_{double,measured}$, can be obtained by least squares regression:

$$\Delta p_{t,1-2} = \mathrm{C}_{double,measured} \cdot p_v = \mathrm{C}_{double,measured} \cdot \frac{\rho}{2}\left(\frac{Q}{A}\right)^2 \qquad (6)$$

Meanwhile, the loss coefficient of the double bends with the intermediate duct as a whole resistance component was calculated from the friction factor for straight duct in the relaxed positioned, f_{relax}, and the loss coefficient of a single bend at 90°, C_{90^o}, obtained as described in Sections 2.1 and 2.2:

$$\mathrm{C}_{double,calculated} = \mathrm{C}_{90^o} + f_{relax} \cdot \frac{L_{in}}{D} + \mathrm{C}_{90^o} \qquad (7)$$

where L_{in} is the length of the intermediate duct. The $\mathrm{C}_{double,calculated}$ was then compared with the $\mathrm{C}_{double,measured}$. If the error between the calculated and measured data was small, the influence of the intermediate duct could be neglected, and the two bends could be considered separately. Table 3 lists the case setup details for the measurements of pressure drop in double-bend flexible ducts. The tested length of the intermediate duct ranged from $2D$ to $16D$.

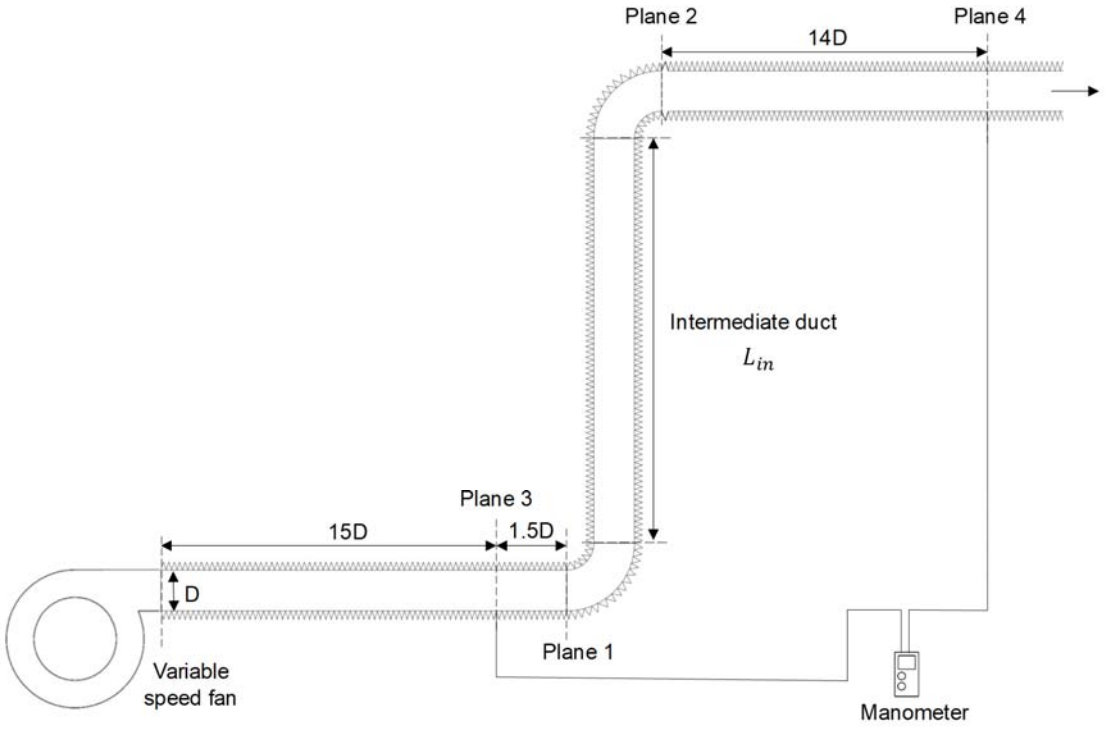

Figure 4. Schematic of the experimental setup for measuring the pressure drop in a double-bend flexible duct.

Table 3. Case setup for the double-bend flexible ducts.

Case No.	Duct inner diameter, D (mm)	Average air velocity, $V = Q/A$ (m/s)	Intermediate duct length, L_{in} (mm)
1	52	4 to 10	2D
2	52	4 to 10	4D
3	52	4 to 10	6D
4	52	4 to 10	8D
5	52	4 to 10	10D
6	52	4 to 10	12D
7	52	4 to 10	14D
8	52	4 to 10	16D
9	36	4 to 10	4D
10	36	4 to 10	6D
11	36	4 to 10	8D
12	36	4 to 10	10D
13	36	4 to 10	12D

3. Results

3.1 Straight flexible duct

In Figure 5, the pressure differential, $\Delta p_{straight,1-2}$, is plotted against the term $\frac{L}{D}\frac{\rho}{2}(\frac{Q}{A})^2$ according to Eq. (2) for the straight flexible duct with inner diameter of 52 mm under different compression ratios. For air velocity, each measurement was conducted for six times and the standard deviations ranged from 0.12 to 0.85 m/s. For pressure differential, the measurement uncertainties were within 1 Pa, which was applicable to all the pressure differential measurements in this study. All the results exhibit good linearity, with an R^2 greater than 0.94. Based on Eq. (2), the slope can be regarded as the friction factor for the straight flexible duct. It can be seen that the friction factor, f, decreased with the compression ratio, R. As shown in Figure 2, when the flexible duct was fully stretched ($R = 1$), the peaks and valleys tended to be flatter than those for the compressed ducts ($R < 1$). Namely, a flatter surface tended to represent a lesser roughness, which would lead to lower air resistance. Thus, the corresponding friction factor was smaller. Figure 6 is analogous to Figure 5, but for the straight flexible duct with inner diameter of 36 mm. Four compression ratios, 1 (fully stretched), 0.95, 0.916 (relaxed position), and 0.88 (fully compressed), were tested. Each air velocity was conducted for six times and the standard deviations ranged from 0.09 to 0.45 m/s. The general trend was similar to that shown in Figure 5.

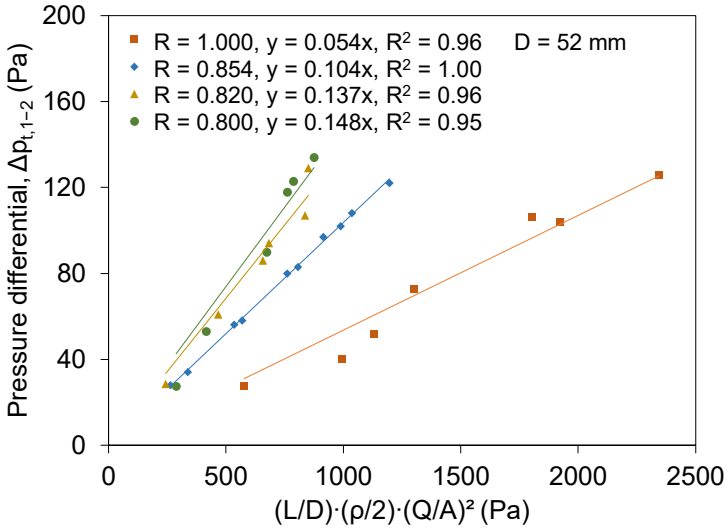

Figure 5. Relationship between the pressure drop in the straight flexible duct with inner diameter of 52 mm and the term $\frac{L}{D}\frac{\rho}{2}(\frac{Q}{A})^2$ when the compression ratio was 1 (fully stretched), 0.854 (relaxed position), 0.82, and 0.8 (fully compressed). The slope was the friction factor, f.

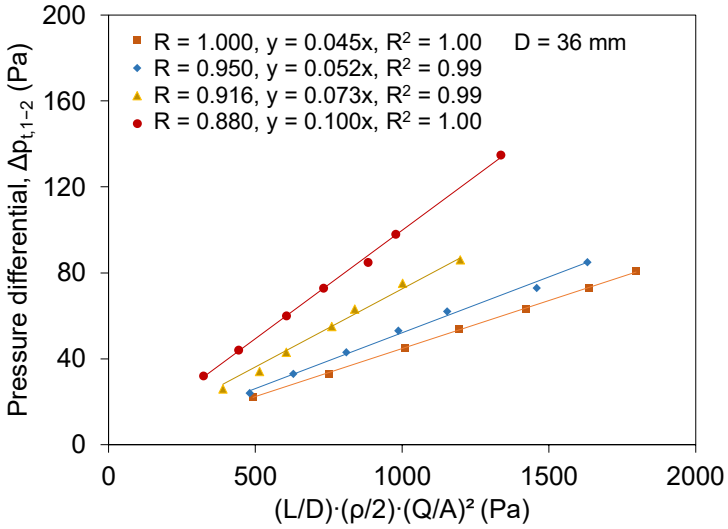

Figure 6. Relationship between the pressure drop in the straight flexible duct with inner diameter of 36 mm and the term $\frac{L}{D}\frac{\rho}{2}(\frac{Q}{A})^2$ when the compression ratio was 1 (fully stretched), 0.95, 0.916 (relaxed position), and 0.88 (fully compressed). The slope was the friction factor, f.

Figure 7(a) and (b) depict the relationship between the friction factor and compression ratio for the straight flexible ducts with inner diameters of 52 and 36 mm, respectively. Again, the friction factor decreased with the compression ratio. For the 52-mm duct, the friction factor increased from 0.104 to 0.148, i.e., by 42.3%, when the duct initially in the relaxed position was fully compressed. For the 35-mm flexible duct, the increase was 37.0%, from 0.073 to

0.100. It was found that the exponential function fitted well with the data for both flexible ducts, as shown in Figure 7. The empirical equations can be used to predict the friction factor of the straight flexible duct under other compression ratios.

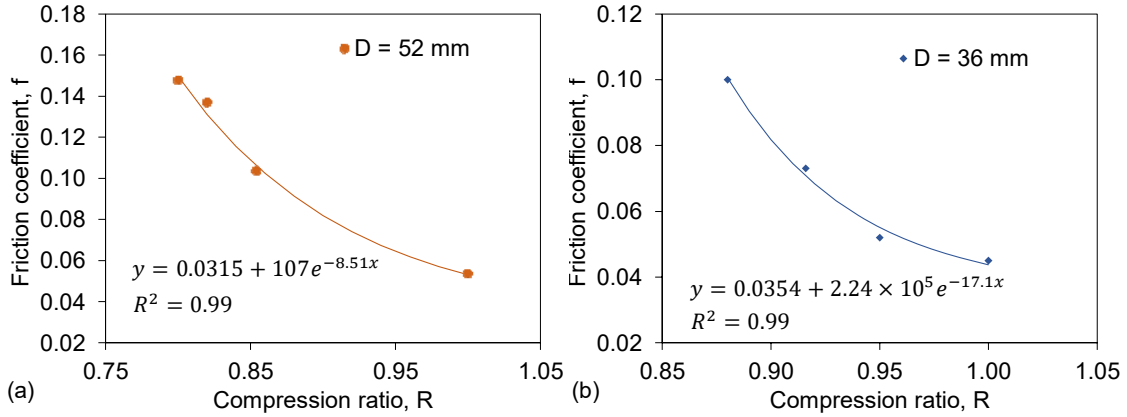

Figure 7. Relationship between the friction factor and compression ratio for the straight flexible ducts with inner diameters of (a) 52 mm and (b) 36 mm.

For the sake of comparison, this study also conducted measurements for a regular PVC duct without peaks and valleys. The diameter of the PVC duct was 52 mm. Figure 8 compares the measured pressure drop in the regular PVC duct with that in the fully stretched and fully compressed 52-mm flexible duct. For the PVC duct, each air velocity was conducted for six times and the standard deviations ranged from 0.14 to 0.18 m/s. The friction factor for the fully stretched flexible duct was found to be 116% higher than that for the PVC duct, and the friction factor for the fully compressed flexible duct was 492% higher. Therefore, although flexible ducts can provide more flexibility for installation, the pressure drop, likes the fan energy, tends to be greater than for regular ducts.

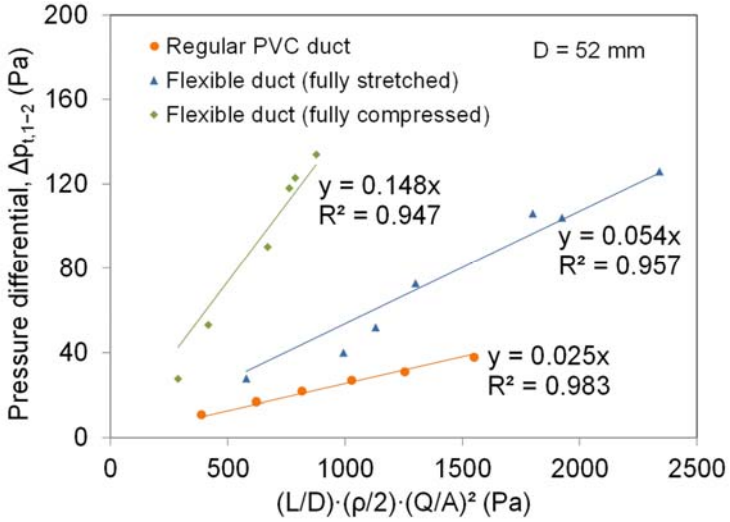

Figure 8. Comparison of the measured pressure drop in the regular PVC duct with that in the fully stretched and fully compressed flexible duct.

Note that the outer diameter would also influence the geometry of the peaks and valleys, which consequently would affect the air resistance of the flexible duct. This is similar to the compression which influences the geometry of the peaks and valleys, and so as the air resistance. Therefore. one can get some insights from the results with different compression ratios. The experimental results show that the air resistance increased when the flexible duct was compressed. Also, when the flexible duct was compressed, the outer diameter became greater. Therefore, the air resistance would increase with a greater outer diameter. It should also be noted that, for other types of flexible ducts with different outer diameters at the relaxed position, additional experiments should be conducted to obtain the corresponding measured data using the methods described in this study.

3.2 Bent flexible duct

For the bent flexible ducts, the pressure differential across the bend, i.e., $\Delta p_{t,1-2}$, was obtained from the measurements and Eq. (4). In Figure 9, the pressure differential, $\Delta p_{t,1-2}$, is plotted against the dynamic pressure, p_v, for the 52-mm flexible duct at bending angles of 30º, 60º, 90º, 120º, and 150º. For air velocity, each measurement was conducted for six times and the standard deviations ranged from 0.14 to 0.40 m/s. All the results exhibit good linearity, with an R^2 greater than 0.93. According to Eq. (5), the slope of the regression can be regarded as the loss coefficient, C, of the bend. It can be seen that the loss coefficient increased with the bending angle, as a larger degree of bending tended to increase the local air resistance. Figure 10 is analogous to Figure 9, but for the 36-mm flexible duct. Each air velocity was conducted for six times and the standard deviations ranged from 0.14 to 0.31 m/s. The two figures reveal similar trends for both duct sizes.

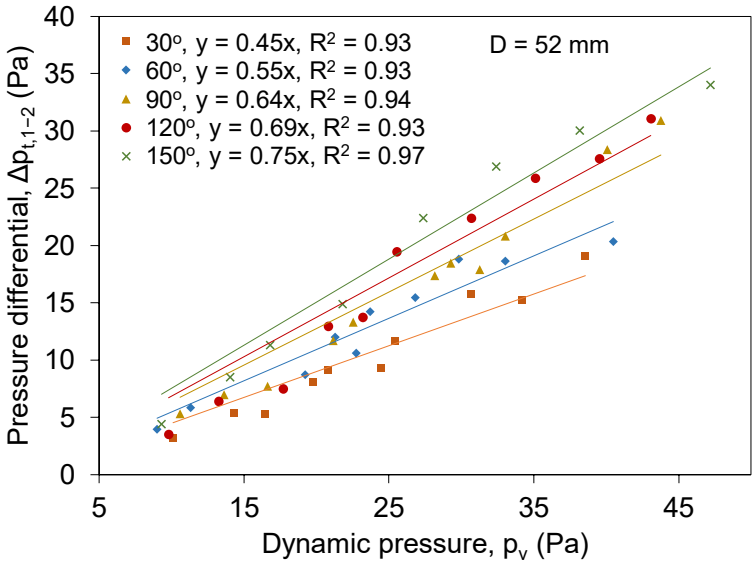

Figure 9. Relationship between the pressure drop across the bend and the dynamic pressure for the 52-mm bent flexible duct at bending angles of 30º, 60º, 90º, 120º, and 150º. The slope is the loss coefficient of the bend, C.

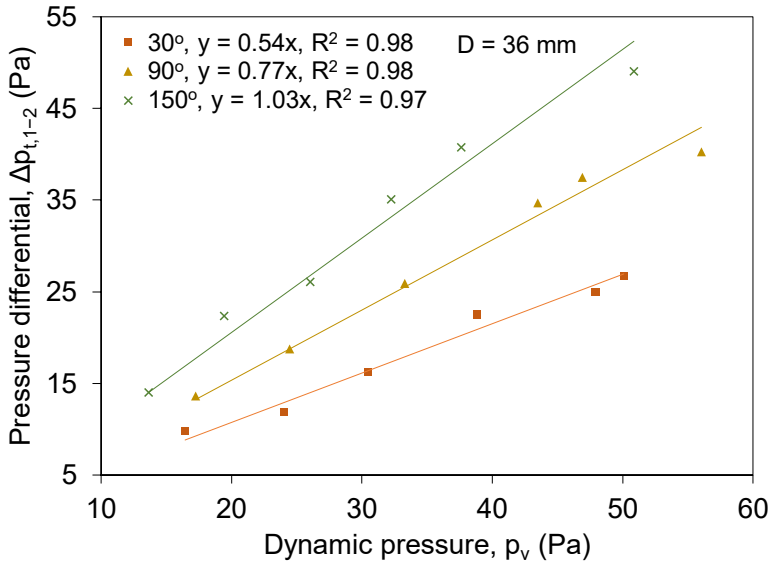

Figure 10. Relationship between the pressure drop across the bend and the dynamic pressure for the 36-mm bent flexible ducts at bending angles of 30º, 90º, and 150º. The slope is the loss coefficient of the bend, C.

Figure 11 further plots the loss coefficient of the bend as a function of bending angle for both flexible ducts. Again, the loss coefficient increased with the bending angle. For the 52-mm duct, when the bending angle increased from 30º to 150º, the loss coefficient increased from 0.45 to 0.75, i.e., by 66.7%. For the 36-mm duct, the increase was 90.7%, from 0.54 to 1.03. The half-life exponential function fitted the experimental data well, with an R^2 greater than 0.99. The empirical equations can be used to predict the loss coefficient of bends with different angles. Furthermore, the loss coefficients of the 36-mm bends were greater than those of the 52-mm bends. This was because a smaller size was usually associated with greater air resistance. The results indicate that a large degree of bending should be avoided in the installation of flexible ventilation ducts in order to reduce the pressure loss.

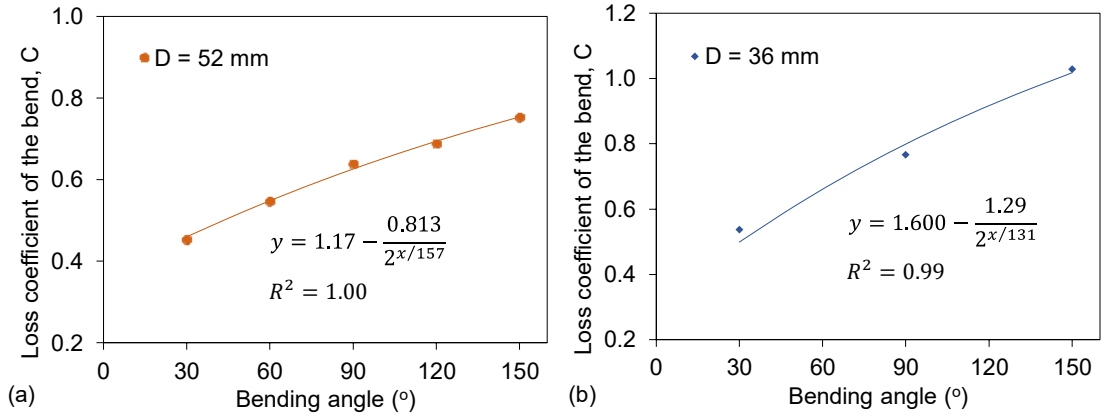

Figure 11. Relationship between pressure drop coefficient and bending angle for bent flexible ducts with diameters of 52 and 36 mm.

3.3 Double-bend flexible duct

For a flexible ducting system, the total pressure drop can be calculated from the friction factors for straight flexible ducts and the loss coefficients of the bends, obtained as described above. However, if the intermediate duct length between two bends is too short, the calculated total pressure drop may not be accurate. Therefore, this study conducted experiments with double-bend flexible ducts to explore the influence of the intermediate duct length on the calculated total pressure drop. Figure 12 plots the pressure differential, $\Delta p_{t,1-2}$, calculated according to Eq. (6) for the 52-mm double-bend flexible duct as defined in Figure 4, against the dynamic pressure under different intermediate duct lengths ranging from $2D$ to $16D$. For air velocity, each measurement was conducted for six times and the standard deviations ranged from 0.09 to 0.34 m/s. The slope represents the loss coefficient of the double bends with the intermediate duct as a whole resistance component, $C_{double,measured}$. Obviously, with the increase in the intermediate duct length, the loss coefficient also increased. Figure 13 is analogous to Figure 12 but for the 36-mm double-bend flexible ducts. Each air velocity was conducted for six times and the standard deviations ranged from 0.14 to 0.31 m/s. The general trend was similar to that for the 52-mm double-bend ducts. These measured loss coefficients, $C_{double,measured}$, will be used as the benchmark for comparison in the following sub-section.

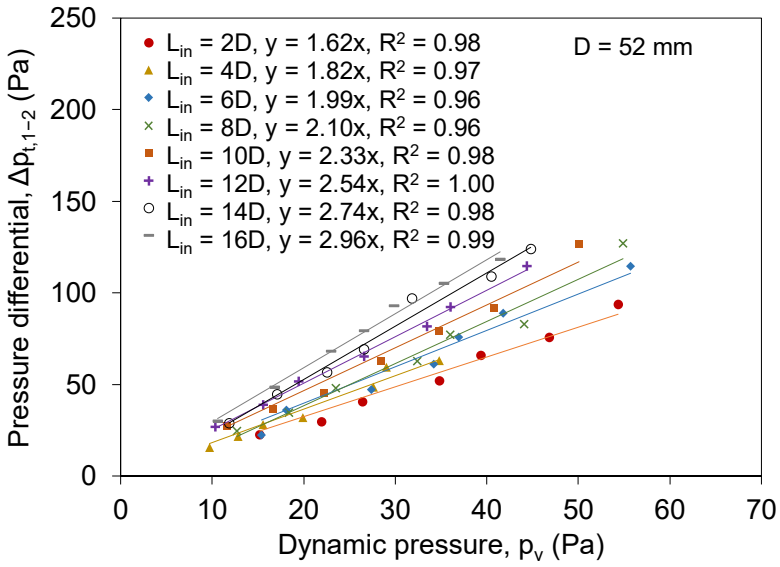

Figure 12. Relationship between the pressure drop across the double bends with the intermediate duct as a whole resistance component and the dynamic pressure, for the 52-mm double-bend flexible ducts with intermediate duct length ranging from $2D$ to $16D$. The slope was the loss coefficient, $C_{double,measured}$.

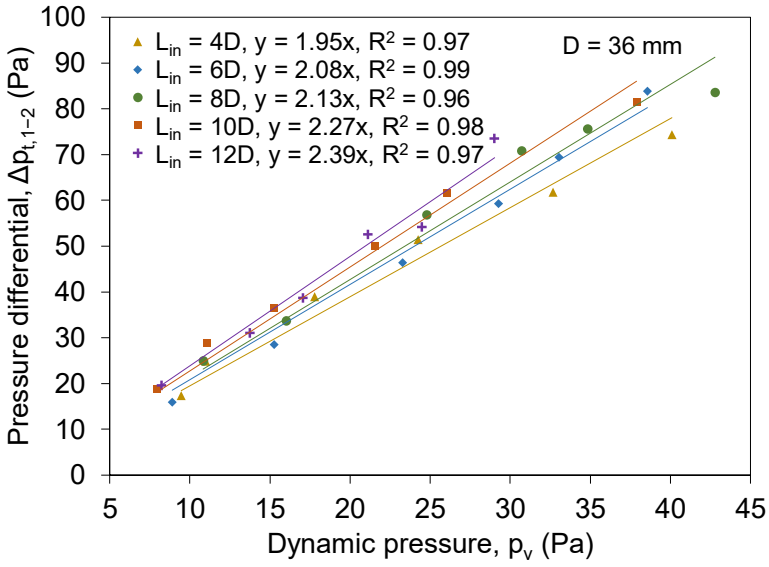

Figure 13. Relationship between the pressure drop across the double bends with the intermediate duct as a whole resistance component and the dynamic pressure, for the 36-mm double-bend flexible ducts with intermediate duct length ranging from $4D$ to $12D$. The slope was the loss coefficient, $C_{double,measured}$.

The loss coefficient can also be calculated from the friction factor for a straight duct in the relaxed position, f_{relax}, and the loss coefficient of a single bend at 90°, C_{90^o}, according to Eq. (7). If the calculated loss coefficient, $C_{double,calculated}$, was similar to the measured data, $C_{double,measured}$, it would indicate that the intermediate duct was sufficiently long, and the pressure drop across the two bends could be calculated separately from the loss coefficients of the individual bends. Figure 14 compares the loss coefficient across the double bends with the intermediate duct as a whole resistance component, as measured in the experiments and as calculated by Eq. (7). For the 52-mm double-bend flexible ducts, when the intermediate duct length was greater than or equal to $8D$, the relative errors of the calculated loss coefficients compared with the measured data were smaller than 1%. Similar results were found for the 36-mm double-bend ducts. Therefore, if an accuracy within 1% is to be achieved for the calculation using Eq. (7), the length of the intermediate duct should be greater than or equal to $8D$. Furthermore, if the tolerance of relative error is 10%, the length of intermediate duct can be as short as $2D$.

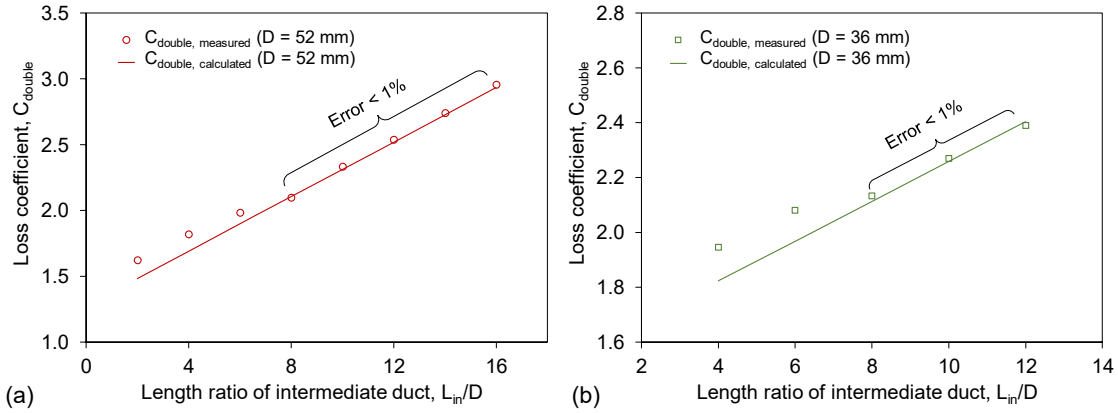

Figure 14. Comparison of the loss coefficient across the double bends with the intermediate duct as a whole resistance component, as measured in the experiments and as calculated by Eq. (7).

4. Practical implications

According to the experimental results, the friction factor increased with a decrease in compression ratio. Furthermore, compressing a flexible duct may raise the chance of bending the duct, as shown in Figure 15(a). Therefore, in the installation of flexible ventilation ducts, excessive compression should be avoided. In many real applications, flexible ducts are not well supported, as illustrated by Figure 15(b). Unsupported flexible ducts tend to have multiple bends, which would lead to increased pressure drop. Therefore, flexible ventilation ducts should be well supported to reduce the number of bends, and hence the pressure drop, during installation. Moreover, in real applications, the engineers who install flexible ventilation ducts are not the ones who designed them. In some cases, even though the design of a ducting system is reasonable, excessive bending may still occur, as it may make the installation easier. Therefore, extra attention should be paid during installation to avoid excessive bending, and thus excessive pressure loss.

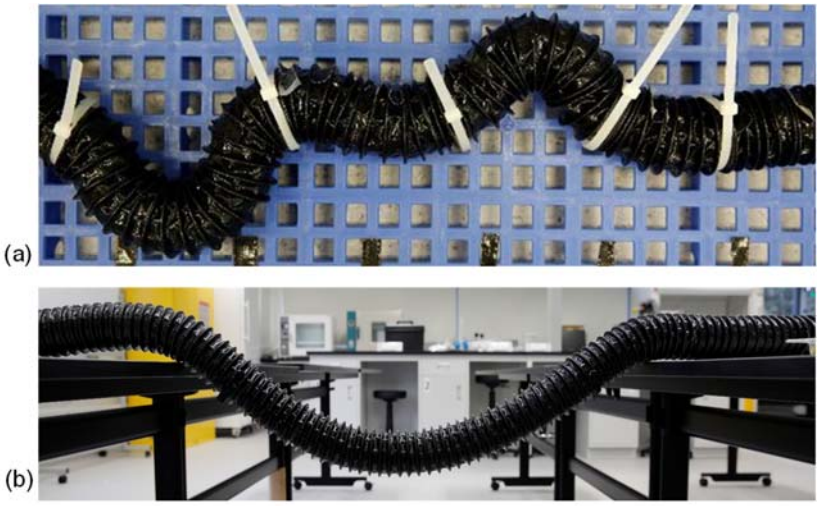

Figure 15. Photographic images of (a) a compressed flexible duct with multiple bends and (b) a flexible duct without support, leading to multiple bends.

With the experimental data obtained in this study, the total pressure drop in a flexible duct with multiple bends and multiple straight sections can be calculated. As an example, this investigation calculated the total pressure drop in a branch of a flexible ducting system shown in Figure 16. The flexible duct with an inner diameter of 36 mm was used to connect the main rigid duct to the supply air nozzle in the ventilation system of an airplane. Due to the limited space and complex geometry in the airplane, there were multiple bends for the flexible duct. The air velocity in the duct was set at 7 m/s. To calculate the total pressure drop, the whole flexible duct was divided to five straight sections and four bends as labelled in Figure 16. Table 4 lists the length and compression ratio of each straight section. According to the results in Figure 7(b), the friction factor for each straight section was calculated based on the compression ratio. The pressure drop in each straight section was then calculated by Eq. (2) based on the diameter, length, air velocity, and friction factor. Furthermore, Table 5 lists the bending angle of each bend. According to the results in Figure 11(b), the loss coefficient for each bend was calculated based on the bending angle. The pressure drop in each bend was then calculated by Eq. (5) based on the air velocity and loss coefficient. Note that the loss coefficient was independent from the compression ratio as the bends could hardly be compressed or stretched. Finally, the total pressure drop in the whole flexible duct was the sum of the pressure drop in each straight section and bend, i.e. 223.01 Pa, in this case. This example demonstrated how the results obtained in this study could be used in real applications.

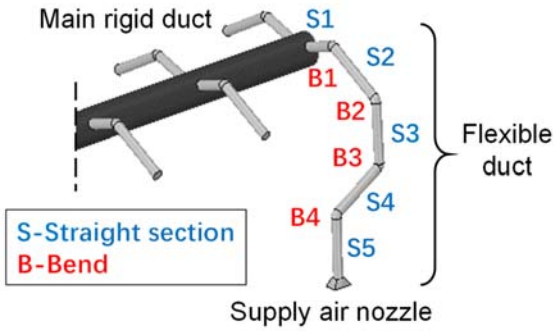

Figure 16. Schematic of a flexible duct with multiple bends and multiple straight sections used in the ventilation system of an airplane.

Table 4. Calculated pressure drop in the each straight section of the flexible duct.

No.	Diameter (m)	Length (m)	Air velocity (m/s)	Compression ratio	Friction factor	Pressure drop (Pa), ΔP_m
S1	0.036	0.2	7.00	0.85	0.144	23.28
S2	0.036	0.5	7.00	0.90	0.082	32.95
S3	0.036	0.3	7.00	0.90	0.082	19.77
S4	0.036	0.5	7.00	0.90	0.082	32.95
S5	0.036	0.4	7.00	0.85	0.144	46.57
Sum						155.52

Table 5. Calculated pressure drop in each bend of the flexible duct.

No.	Diameter (m)	Bending angle (°)	Air velocity (m/s)	Loss coefficient	Pressure drop (Pa), ΔP_j
B1	0.036	30	7.00	0.499	14.48
B2	0.036	45	7.00	0.583	16.92
B3	0.036	60	7.00	0.661	19.17
B4	0.036	45	7.00	0.583	16.92
Sum					67.49

In practical applications, if a flexible duct with a different diameter or different "peaks and valleys" geometry is used, experimental measurements should be conducted to obtain the corresponding friction factors and loss coefficients. With the measured friction factors and loss coefficients, the pressure drop across this type of flexible duct with multiple bends and multiple straight sections can be calculated as demonstrated in the example above. Although the data presented in this paper cannot cover all the possible cases, the methods proposed in this study can be used to measure the friction factors and loss coefficients and to calculate the total pressure drop across the flexible duct with multiple bends and multiple straight sections. Theoretically, CFD can be used for calculating the airflow and pressure distribution without the need of experimental measurements (e.g. Agirman et al. 2020; Chen et al. 2016; Liu et al. 2019; Mutlu 2020; Pan et al. 2019). However, the "peaks and valleys" geometry of flexible ducts can be very complex and would result in a large number of grids. The complex geometry and large grid number would significantly influence the accuracy of the calculations and increase the computing time. Therefore, the proposed methods in this study may be more suitable for practical applications.

5. Conclusions

This study conducted experimental measurements of the pressure drop across flexible ventilation ducts under different compression ratios and bending angles. The friction factors were obtained for the straight flexible ducts. The loss coefficients of the bends were also measured for single-bend flexible ducts. Finally, the influence of the intermediate duct length on the pressure drop across two bends was experimentally investigated. The data obtained in this study can be used for the calculations of total pressure loss in flexible ventilation ducting systems in buildings. Within the scope of this research, the following conclusions can be made:

1. The friction factor for the straight flexible ducts was negatively associated with the compression ratio.
2. The loss coefficient of the bend increased with the bending angle for single-bend flexible ducts.
3. When the length of the intermediate duct was greater than $8D$, the pressure drop across a double-bend flexible duct could be calculated from the friction factors and loss coefficients with a relative error less than 1%.

Acknowledgement

This work was partially supported by the Early Career Scheme of Research Grants Council of Hong Kong SAR, China (Grant No. 24208518 and 25210419) and the National Natural Science Foundation of China (Grant No. 51708474).

References

Abushakra B, Walker I, Sherman M (2004). Compression effects on pressure loss in flexible HVAC ducts. *HVAC&R Research*, 10: 275-289.

Agirman A, Cetin YE, Avci M, Aydin O (2020). Effect of air exhaust location on surgical site particle distribution in an operating room. *Building Simulation*, 13: 979-988.

American Society of Heating, Refrigerating and Air-Conditioning Engineers (2005). I-P & SI Handbook-Fundamentals, Table 1, p.35.7.

American Society of Heating, Refrigerating and Air-Conditioning Engineers (2017). Standard 120-2017: Method of testing to determine flow resistance of Hvac ducts and fittings.

Brown GO (2002). Henry Darcy and the making of a law. *Water Resources Research*, 38: 1-12.

Chen C, Zhang X, Groll E, McKibben A, Long N, Dexter M, Chen Q (2016). A method of assessing the energy cost saving from using an effective door closer. *Energy and Buildings*, 118: 329-338.

Chen H, Cai WJ, Chen C (2016). Model-based method for testing, adjusting and balancing of HVAC duct system. *Energy and Buildings*, 126: 498-507.

Culp C (2011). HVAC flexible duct pressure loss measurements. *ASHRAE Research Project RP-1333 final report*.

Culp C, Cantrill D (2009). Static pressure losses in 12", 14", and 16" non-metallic flexible ducts with compression and sag. *ASHRAE Transactions*, 115: 622-628.

Du X, Wei A, Fang Y, Yang Z, Jin Z (2020). The effect of bend angle on pressure drop and flow behavior in a corrugated duct. *Acta Mechanica*, 231: 3755-3777.

Gibbs DC, Idem S (2010). Measured and predicted pressure loss in corrugated spiral duct. *ASHRAE Transactions*, 116: 380-386.

Griggs EI, Khodabakhsh-Sharifabad F (1992). Flow characteristics in rectangular ducts. *ASHRAE Transactions*, 98: 116-127.

Griggs EI, Swim WB, Henderson GH (1987). Resistance to flow of round galvanized ducts. *ASHRAE Transactions*, 93: 3-16.

Hodges RK ,Kulkarni D, Idem S (2013). Pressure loss in fully stretched nonmetallic flexible duct with a bend. *HVAC&R Research*, 19: 87-100.

Huebscher RG (1948). Friction equivalents for round, square and rectangular ducts. *ASHVE Transactions*, 54: 101-118.

Kokayko M, Jolton J, Beggs T, Walthour TS, Dickson B (1996). Residential Ductwork and Plenum Box Bench Tests. *IBACOS Burt Hill Project 95006*.

Kulkarni D, Khaire S, Idem S (2009). Pressure loss of corrugated spiral duct. *Ashrae Transactions*, 115: 28-34.

Kulkarni D, Idem S (2015). Loss coefficients of bends in fully stretched nonmetallic flexible ducts. *Science and Technology for the Built Environment*, 21: 413–419.

Mutlu M (2020). Numerical investigation of indoor air quality in a floor heated room with different air change rates. *Building Simulation*, 13: 1063-1075.

Mylaram NK, Idem S (2005). Pressure Loss Coefficient Measurements of Two Close-Coupled HVAC Elbows. *HVAC&R Research*, 11: 133-146.

Nalla AN, Idem S (2012). Laboratory testing of saddletap tees to determine loss coefficients. *ASHRAE Transactions*, 118: 1131-1145.

Ojima J (2017). Decline of the performance of a portable axial-flow fan due to the friction and duct bending loss of a connected flexible duct. *Journal of Occupational Health*, 59: 210-213.

Pan Y, Lin C-H, Wei D, Chen C (2019). Experimental measurements and large eddy simulation of particle deposition distribution around a multi-slot diffuser. *Building and Environment*, 150: 156-163.

Paruchuri A, Idem S (2018). Experimental comparison of pressure loss in typical flexible and sheet metal residential duct systems. *ASHRAE Transactions*, 124: 102-115.

Salehi M, Sleiti AK, Idem S (2017). Study to identify computational fluid dynamics models for use in determining HVAC duct fitting loss coefficients. *Science and Technology for the Built Environment*, 23: 181-191.

Sun Y, Ford SE, Zhang Y (2015). Laboratory testing of flat oval transitions to determine loss coefficients (RP-1606). *Science and Technology for the Built Environment*, 21: 386-395.

Townsend B, Khodabakhsh-Sharifabad F, Idem S (1996). Loss coefficient measurements for flat oval elbows and transitions. *ASHRAE Transactions*, 102: 159-169.

Weaver K, Culp C (2007). Static pressure losses in nonmetallic flexible duct (6", 8", and 10"). *ASHRAE Transactions*, 113: 400-405.

Liu W, You R, Chen C (2019). Modeling transient particle transport by fast fluid dynamics with the Markov chain method. *Building Simulation*, 12: 881–889.